PNAS
www.pnas.org

# Supplementary Information for

## The neural signature of the decision value of future pain

**MP Coll, H Slimani, CW Woo, TD Wager, P Rainville, E Vachon-Presseau & M Roy**

**Corresponding author: Mathieu Roy**
**E-mail: mathieu.roy3@mcgill.ca**

**This PDF file includes:**

Supplementary text
Figs. S1 to S12
Table S1 to S3
SI References

# Supporting Information Text

## Supplementary methods

**Instructions for the behavioural task.** You will now undergo the main task of the experiment in which the computer will make offers that include money and pain and you will have to simply accept or decline the offers. The computer is set so that the maximum pain the computer will offer will not be above the tolerance level we set in the previous calibration. At the end of the experiment, the computer will randomly select 10 trials out of all the trials you performed and you will receive the amount of money in these 10 trials if you accepted the offer. In other words, if you accept the offer, you have a chance to receive the money attached to this offer at the end of the experiment. If you decline an offer, it is impossible to get the money attached. If a declined trial is selected randomly at the end of the experiment, you will receive no money for this trial. You should therefore make punctual choices at each trial ("Do I want this shock for that amount of money?") and answer according to your desire at this moment. You should not try to adopt a strategy or try to calculate how much money you might gain: it is impossible to guess. The offers the computer makes come in a randomized order, but they are predetermined. Your answers therefore have no impact on the subsequent offers that the computer will make. Also, whether you accept or decline the offers does not affect the results of the experiment. As long as you answer punctually and honestly, we will have a good data set. *Run the two practice trials and ask them to answer "Yes" to the first trial and explain that this would lead to a shock and "No" to the second trial and that this would not lead to a shock but that they would lose the opportunity to gain the money.*

**fMRI and MRI data preprocessing.** *This section was automatically generated by fMRIPrep 20.1.1.* Results included in this manuscript come from preprocessing performed using *fMRIPrep* 20.1.1 (1; 2; RRID:SCR_016216), which is based on *Nipype* 1.5.0 (3; 4; RRID:SCR_002502).

***Anatomical data preprocessing.*** A total of 1 T1-weighted (T1w) images were found within the input BIDS dataset. The T1-weighted (T1w) image was corrected for intensity non-uniformity (INU) with N4BiasFieldCorrection (5), distributed with ANTs 2.2.0 (6, RRID:SCR_004757), and used as T1w-reference throughout the workflow. The T1w-reference was then skull-stripped with a *Nipype* implementation of the antsBrainExtraction.sh workflow (from ANTs), using OASIS30ANTs as target template. Brain tissue segmentation of cerebrospinal fluid (CSF), white-matter (WM) and gray-matter (GM) was performed on the brain-extracted T1w using fast (FSL 5.0.9, RRID:SCR_002823, 7). Volume-based spatial normalization to one standard space (MNI152NLin2009cAsym) was performed through nonlinear registration with antsRegistration (ANTs 2.2.0), using brain extracted versions of both T1w reference and the T1w template. The following template was selected for spatial normalization: *ICBM 152 Nonlinear Asymmetrical template version 2009c* [8, RRID:SCR_008796; TemplateFlow ID: MNI152NLin2009cAsym].

***Functional data preprocessing.*** For each of the 5 BOLD runs found per subject (across all tasks and sessions), the following preprocessing was performed. First, a reference volume and its skull-stripped version were generated using a custom methodology of *fMRIPrep*. Head-motion parameters with respect to the BOLD reference (transformation matrices, and six corresponding rotation and translation parameters) are estimated before any spatiotemporal filtering using mcflirt (FSL 5.0.9, 9). BOLD runs were slice-time corrected using 3dTshift from AFNI 20160207 (10, RRID:SCR_005927). A B0-nonuniformity map (or *fieldmap*) was estimated based on a phase-difference map calculated with a dual-echo GRE (gradient-recall echo) sequence, processed with a custom workflow of *SDCFlows* inspired by the epidewarp.fsl script and further improvements in HCP Pipelines (11). The *fieldmap* was then co-registered to the target EPI (echo-planar imaging) reference run and converted to a displacements field map (amenable to registration tools such as ANTs) with FSL's fugue and other *SDCflows* tools. Based on the estimated susceptibility distortion, a corrected EPI (echo-planar imaging) reference was calculated for a more accurate co-registration with the anatomical reference. The BOLD reference was then co-registered to the T1w reference using flirt (FSL 5.0.9, 12) with the boundary-based registration (13) cost-function. Co-registration was configured with nine degrees of freedom to account for distortions remaining in the BOLD reference. The BOLD time-series (including slice-timing correction when applied) were resampled onto their original, native space by applying a single, composite transform to correct for head-motion and susceptibility distortions. These resampled BOLD time-series will be referred to as *preprocessed BOLD in original space*, or just *preprocessed BOLD*. The BOLD time-series were resampled into standard space, generating a *preprocessed BOLD run in MNI152NLin2009cAsym space*. First, a reference volume and its skull-stripped version were generated using a custom methodology of *fMRIPrep*. Several confounding time-series were calculated based on the *preprocessed BOLD*: framewise displacement (FD), DVARS and three region-wise global signals. FD was computed using two formulations following Power (absolute sum of relative motions, 14) and Jenkinson (relative root mean square displacement between affines, 9). FD and DVARS are calculated for each functional run, both using their implementations in *Nipype* (following the definitions by 14). The three global signals are extracted within the CSF, the WM, and the whole-brain masks. Additionally, a set of physiological regressors were extracted to allow for component-based noise correction (*CompCor*, 15). Principal components are estimated after high-pass filtering the *preprocessed BOLD* time-series (using a discrete cosine filter with 128s cut-off) for the two *CompCor* variants: temporal (tCompCor) and anatomical (aCompCor). tCompCor components are then calculated from the top 5% variable voxels within a mask covering the subcortical regions. This subcortical mask is obtained by heavily eroding the brain mask, which ensures it does not include cortical GM regions. For aCompCor, components are calculated within the intersection of the aforementioned mask and the union of CSF and WM masks calculated in T1w space, after their projection to the native space of each functional run (using the inverse BOLD-to-T1w transformation). Components are also calculated separately within the WM and CSF masks. For each CompCor decomposition, the *k* components with the largest singular values are retained, such that the retained components' time series are sufficient to explain 50 percent of variance across the nuisance mask (CSF, WM, combined, or temporal). The remaining components are dropped from consideration. The head-motion estimates

calculated in the correction step were also placed within the corresponding confounds file. The confound time series derived from head motion estimates and global signals were expanded with the inclusion of temporal derivatives and quadratic terms for each (16). Frames that exceeded a threshold of 0.5 mm FD or 1.5 standardised DVARS were annotated as motion outliers. All resamplings can be performed with *a single interpolation step* by composing all the pertinent transformations (i.e. head-motion transform matrices, susceptibility distortion correction when available, and co-registrations to anatomical and output spaces). Gridded (volumetric) resamplings were performed using antsApplyTransforms (ANTs), configured with Lanczos interpolation to minimize the smoothing effects of other kernels (17). Non-gridded (surface) resamplings were performed using mri_vol2surf (FreeSurfer). Many internal operations of *fMRIPrep* use *Nilearn* 0.6.2 (18, RRID:SCR_001362), mostly within the functional processing workflow. For more details of the pipeline, see the section corresponding to workflows in *fMRIPrep*'s documentation.

***Copyright Waiver.*** The above boilerplate text was automatically generated by fMRIPrep with the express intention that users should copy and paste this text into their manuscripts *unchanged*. It is released under the CC0 license.

## Supplementary results

**S1 - Detailed behavioural results.** We report the detailed results for each of the mixed-model reported in the main text testing for the effect of pain and money levels and presentation order on choice behavior (Table S1), the effect of pain and money levels, choice and presentation order on response time (Table S2) and the effect of choice difficulty and presentation order on response time (Table S3). We also display the matrices shown in Figure 1 separately for trials in which pain level was presented first and trials in which money level was presented first (Figure S1).

**S2 - Relationship between individual differences in PVP and MVP similarity and behaviour.** To provide additional evidence that the pain value pattern (PVP) and the money value pattern (MVP) are related to participants' behavior, we tested the association between individual differences in PVP and MVP similarity and participant specific's influence of pain and money on choice behavior and response time. Specifically, we obtained participant-level weights of money and pain by performing logistic (choices) or linear (response time) regressions within each participant with pain and money levels as predictors. We then correlated these coefficients with the average PVP and MVP pattern similarity during the offer and decision phases.

For the Offer phase, average PVP similarity was negatively related to both coefficients indicating the weight of pain level on choices ($r(56) = -0.31$, $p = 0.02$, Figure S2a) and response time ($r(56) = -0.34$, $p = 0.01$, Figure S2b). This indicates that, across participants, increased PVP similarity during pain offers is associated with a more negative weight of pain level on choices (predicting rejection) and response times (predicting faster choices for higher pain levels). For the MVP, we did not observe a significant relationship between average pattern similarity during money offers and money level weights on choices ($r(56) = 0.12$, $p = 0.38$, Figure S2c) but there was again negative relationship between pattern similarity and money level weights on response time ($r(56) = -0.30$, $p = 0.03$, Figure S2d).

For the Decision phase, regression weights of pain and money levels on choices was not related to either average PVP similarity ($r(56) = -0.17$, $p = 0.21$, Figure S2e) or MVP similarity ($r = -0.04$, $p = 0.75$, Figure S2g). However, we observed the same negative relationships as in the offer phase between PVP and pain level weight on response time ($r(56) = -0.32$, $p = 0.02$, Figure S2f) and MVP similarity and money level weight on response time ($r(56) = -0.48$, $p < 0.001$, Figure S2g). This pattern of result did not vary as a function of presentation order.

Overall, these results suggest that individual differences in pain and money valuation as measured by their impact on behavior are associated with overall PVP and MVP similarity.

**S3 - Relationship between PVP and computational estimates of pain value.** We additionally assessed the relationship between PVP similarity and participant-specific computational estimates of pain value. To obtain these computational estimates, we followed the same procedure described in 19 to identify the best function to scale pain levels to monetary amounts based on choice behaviour. Here we compared linear, parabolic and exponential scaling functions and used these functions to estimate participant-specific parameters that could best predict choice behaviour using a logistic choice function (see Vogel et al., 2021 for formulas). Using Bayesian model comparison as implemented in the VBA toolbox (20), we identified the exponential scaling function as the best function in most participants (Figure S3a).

We estimated participant-specific exponential scaling parameters (Figure S3b) and used these parameters to obtain estimates of the subjective value of the different pain offers for each participant (Figure S3c). As shown in Figure S3d, pain subjective value estimates were highly correlated with PVP similarity in most participants. Using a linear mixed-model we confirmed a relationship between pain subjective value and PVP similarity during the Offer phase ($B = 135.11$, $Z = 4.75$, $p < 0.001$). During the decision phase, the relationship between pain subjective value and PVP similarity was lower (Figure S3e) but still significant ($B = 38.75$, $Z = 4.50$, $p < 0.001$). Furthermore, the difference between the subjective value of the two options (pain - money) was significantly related to the difference between the PVP and MVP similarity (Figure S3f; $B = 51.25$, $Z = 8.72$, $p < 0.001$).

We additionally trained a multivariate signature that could predict these computational estimates of pain value (z-scored within participants) using the same approach as the one used for the PVP described in the main text. This pattern showed a similar predictive accuracy as the PVP ($r = 0.46$, $R^2 = 0.21$), its weights were highly correlated with the PVP weights

(r = 0.73, Figure S3g). Comparison of the two bootstrap-corrected patterns showed a clear overlap between the weights of the patterns (Figure S3h). By directly relating PVP similarity to subject-specific computational estimates of pain value and the neural signature predicting those estimates, these results provide additional evidence for the idea that the PVP tracks the subjective value of pain.

**S4 - Local prediction of the decision value of future pain.** To test the hypothesis that a distributed whole-brain pattern supports the representation of the decision value of future pain, we assessed whether local patterns of activity could achieve similar predictive performance as the pattern developed on the activity of the whole brain. To this end, we performed the cross-validated predictions of the future pain level in each parcel of a 486 parcels whole-brain parcellation built by combining various cortical and subcortical brain atlases (see 21 for details) and we compared the top-performing parcel to the results obtained using whole-brain prediction. As shown in Figure S4a, the PVP largely outperformed all parcels including the top-performing parcel located in the right dorsal premotor cortex (MNI coordinates XYZ: 23, 6, 66; r = 0.25, RMSE = 2.77, $R^2$ = 0.07; Figure S4d). Next, to assess how many elementary brain regions were necessary to reach an accuracy similar to the whole-brain accuracy, we performed the cross-validated prediction in an expanding mask, starting from the most predictive parcel and adding voxels from the next most predictive parcel at each iteration until the predictive accuracy (Pearson's r between actual and predicted levels) reached its maximum. This analysis indicated that 96 parcels (36 977 voxels) were necessary to achieve maximal accuracy (Figure S4c). Note that the maximum correlation obtained using this procedure is optimistically biased since the feature selection process was not independent of the test process.

To ensure that this advantage of an increased number of parcels was not inevitable due to the much larger number of features used in the prediction, we compared this result with the results from the same analyses performed for the money level involved in each offer. In contrast to the prediction of pain offer levels, a high accuracy was achieved in the top parcel located in the right VS (MNI coordinates XYZ 18, 20, -6; r = 0.50, RMSE = 2.55, $R^2$ = 0.21; Figure S4b). Strikingly, the prediction of monetary amount reached maximal accuracy after only 6 parcels (4310 voxels; Figure S4c) were included in the expanding mask, and these parcels mostly covered the striatal area (Figure S4e). Altogether, these results suggest that, compared to the representation of future rewards, the representation of future pain relies on a distributed pattern not adequately captured by any single region.

**S5 - Response of previously developed pain patterns to shock intensities and pain offers.** Two previously developed pain patterns 1 - the Neurological Pain Signature (NPS; 22), 2 - the Stimulus-Intensity Independent Pain Signature (SIIPS; 23) showed the expected response to increase in shock intensities (Figure S5a). To assess the similarity of the cerebral representation of hypothetical pain with that of experienced pain, we compared the response of these two patterns to changes in the level of pain offered. This indicated that none of the physical pain patterns tracked the pain offer level (Figure S5b-c).

**S6 - Response of the PVP to pain anticipation.** We calculated the similarity of the PVP with the parametric maps during the anticipation of various shock intensities (*Anticipation*, Figure 1a). These analyses indicated that the PVP did not discriminate between different levels of anticipated pain (binomial tests for discrimination of the different levels ps > 0.05, Figure S6).

**S7 - Influence of presentation order on the prediction of participants' decisions.** To rule out potential presentation order effects in the classification of the participants' decisions based on the expression of the PVP and MVP, we applied the SVM classification separately for trials in which the pain intensity was presented first and trials in which the monetary amount was presented first. As shown in Figure S7, similar pattern results were obtained independently of which information was presented first and all classification accuracies remained significant. We also tested if the presentation order could be predicted using the pattern expressions using a linear SVM and all accuracies remained close to chance level (maximum accuracy for the prediction of which information was presented first: 0.52).

**S8 - Univariate analyses.** We considered the univariate effects of the pain and money levels offered, the shock intensity and the anticipation phase. For each effect (pain level, money level, anticipated intensity, shock intensity) and participant, we performed a mass univariate regression between the beta maps from the first level GLM and the levels. The resulting beta coefficients were entered into a group level two-tailed one-sample t-test against 0 at the second level. The resulting t-value maps were thresholded using a threshold of p < 0.05, FWE corrected and are shown in Figures S8-S11.

Additionally, we directly compared the group-level univariate effect sizes and multivariate weights for pain and money levels according to 1) their spatial similarity and 2) their respective capacity to predict pain and money levels and participants' choices. To this end, we first correlated the second-level group-map of the parametric effect size of pain level and money level with the multivariate pain and money patterns respectively. We observed relatively high correlations between univariate effect sizes and multivariate weights (PVP: r = 0.73, MVP: r = 0.55; Figure S12). We also performed the same choice prediction analyses using the univariate maps of the effect sizes for the parametric effect of pain and money level. which indicated that the univariate map of the effect of pain level could not discriminate between choices across participants (balanced accuracy = 0.49, p = 0.06) but the univariate map of the effect of money level could predict choices (balanced accuracy = 0.60, p < 0.001). These results suggest that the multivariate pain pattern possesses a finer-grained representation of pain compared to the univariate pattern that can better discriminate between participants' decisions to accept or reject pain.

**Table S1.** Mixed-effects model results for the effect of pain level, money level and presentation order on acceptance.

| | | Acceptance | |
|---|---|---|---|
| *Predictors* | *Odds Ratios* | *CI* | *p* |
| (Intercept) | 0.16 | 0.08 – 0.33 | <0.001 |
| Pain level | 0.56 | 0.52 – 0.61 | <0.001 |
| Money level | 3.97 | 3.52 – 4.46 | <0.001 |
| Presentation order | 1.08 | 0.89 – 1.29 | 0.437 |
| Pain level*Money level | 0.93 | 0.92 – 0.95 | <0.001 |
| **Random Effects** | | | |
| $\sigma^2$ | 3.29 | | |
| $\tau_{00}$ Subjects | 4.27 | | |
| ICC | 0.56 | | |
| N Subjects | 57 | | |
| Observations | 5685 | | |
| Marginal $R^2$ / Conditional $R^2$ | 0.680 / 0.861 | | |

**Table S2.** Mixed-effects model results for the effect pain level, money level, acceptance and presentation order on response time.

| | | Response time | |
|---|---|---|---|
| *Predictors* | *Estimates* | *CI* | *p* |
| (Intercept) | 831.33 | 681.52 – 981.14 | <0.001 |
| Pain level | -3.17 | -21.72 – 15.37 | 0.737 |
| Money level | 127.13 | 90.60 – 163.65 | <0.001 |
| Acceptance | 391.67 | 197.13 – 586.21 | <0.001 |
| Presentation order | 324.12 | 139.50 – 508.74 | 0.001 |
| Pain level*Money level | -7.67 | -12.28 – -3.05 | 0.001 |
| Pain level*Acceptance | 114.33 | 74.29 – 154.37 | <0.001 |
| Money level*Acceptance | -180.27 | -222.00 – -138.53 | <0.001 |
| Pain level*Presentation order | -46.54 | -72.78 – -20.31 | 0.001 |
| Money level Presentation order | -44.3 | -96.63 – 8.02 | 0.097 |
| Acceptance*Presentation order | -561.46 | -835.38 – -287.54 | <0.001 |
| (Pain level*Money level)*Acceptance | 3.1 | -3.43 – 9.64 | 0.352 |
| (Pain level*Money level)*Presentation order | 4.01 | -2.59 – 10.61 | 0.233 |
| (Pain level*Acceptance)*Presentation order | 48.71 | -6.38 – 103.81 | 0.083 |
| (Money level*Acceptance)*Presentation order | 71.86 | 12.22 – 131.50 | 0.018 |
| (Pain level*Money level*Acceptance) * Presentation order | -4.39 | -13.56 – 4.78 | 0.348 |
| **Random Effects** | | | |
| $\sigma^2$ | 254154.95 | | |
| $\tau_{00}$ Subjects | 79873.15 | | |
| ICC | 0.24 | | |
| N Subjects | 57 | | |
| Observations | 5685 | | |
| Marginal $R^2$ / Conditional $R^2$ | 0.112 / 0.325 | | |

**Table S3.** Mixed-effect model results for the effect of choice difficulty and presentation order on response time.

| | Response time | | |
|---|---|---|---|
| *Predictors* | *Estimates* | *CI* | *p* |
| (Intercept) | 753.36 | 661.03 – 845.68 | <0.001 |
| Choice difficulty | 58.29 | 50.10 – 66.48 | <0.001 |
| Presentation order | -63.18 | -145.80 – 19.45 | 0.134 |
| Choice difficulty*Presentation order | 1.56 | -10.10 – 13.21 | 0.794 |
| **Random Effects** | | | |
| σ2 | 274749.56 | | |
| τ00 Subjects | 76241.83 | | |
| ICC | 0.22 | | |
| N Subjects | 57 | | |
| Observations | 5685 | | |
| Marginal R2 / Conditional R2 | 0.055 / 0.260 | | |

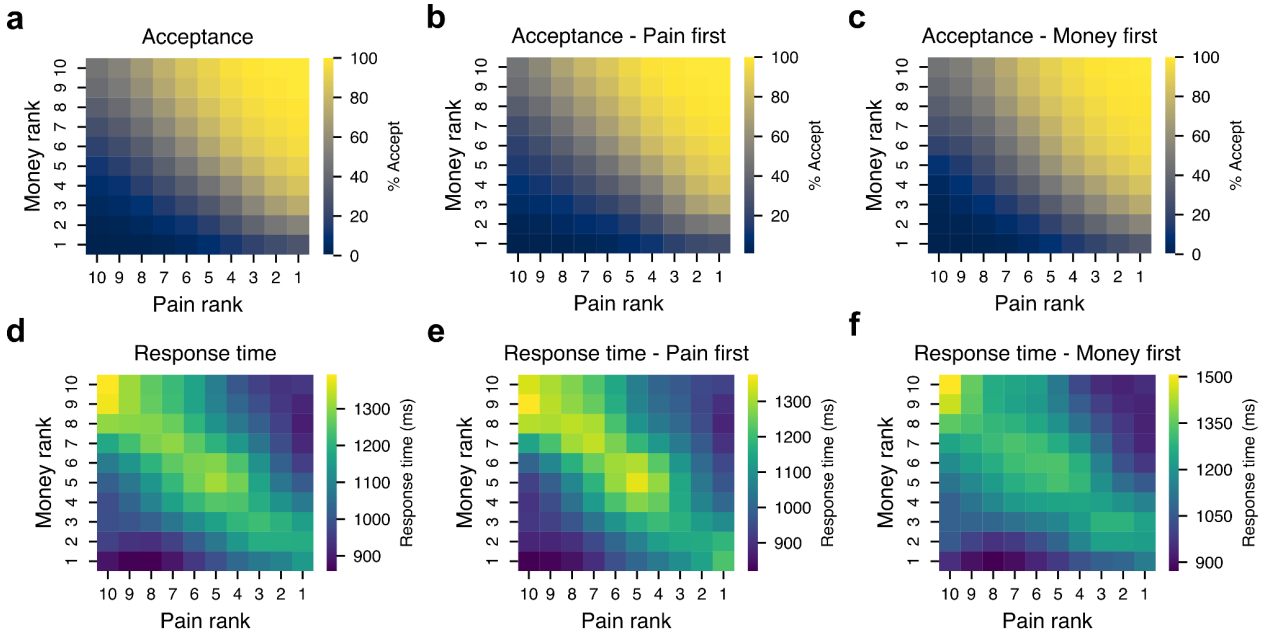


**Fig. S1. Behavioral results as a function of presentation order. (a-c)** The average proportion of offers accepted **(a)** overall **(b)** for trials in which the pain level was presented first and **(c)** for trials in which the money level was presented first. **(d-f)** Average response time as a function of pain and money levels offered **(d)** overall, **(e)** for trials in which the pain level was presented first and **(f)** for trials in which the money level was presented first. Matrices were smoothed with a Gaussian kernel for display only.

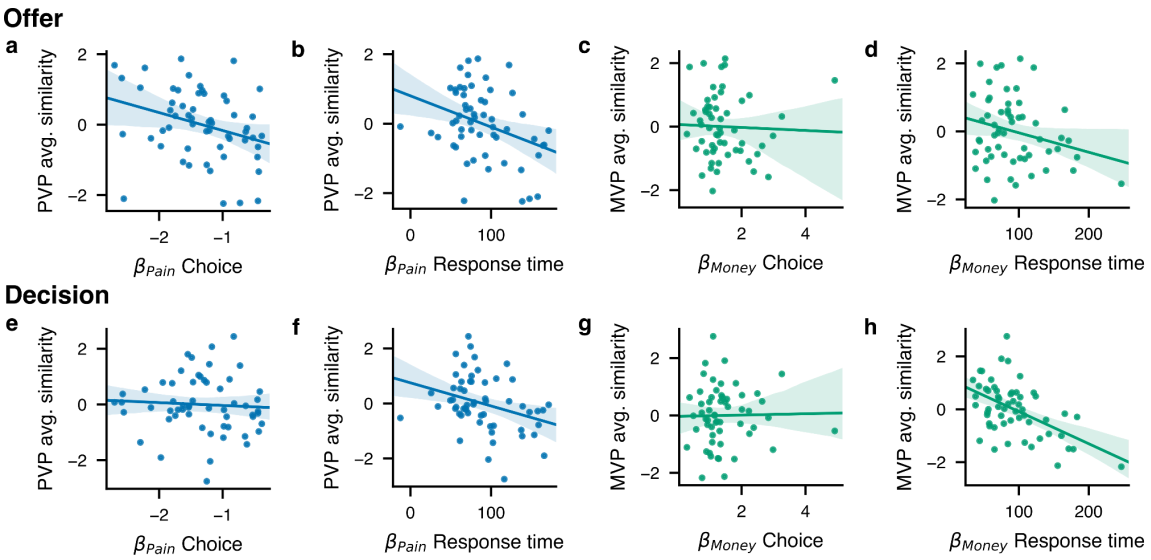


**Fig. S2. Individual differences in behaviour and PVP and MVP similarity. (a-d)** Relationship between average PVP and MVP similarity and beta weights of pain and money levels on response time and choice during the offer phase. **(e-h**) Same but for the decision phase of the task. Pattern similarity values are z-scored across participants for display only.

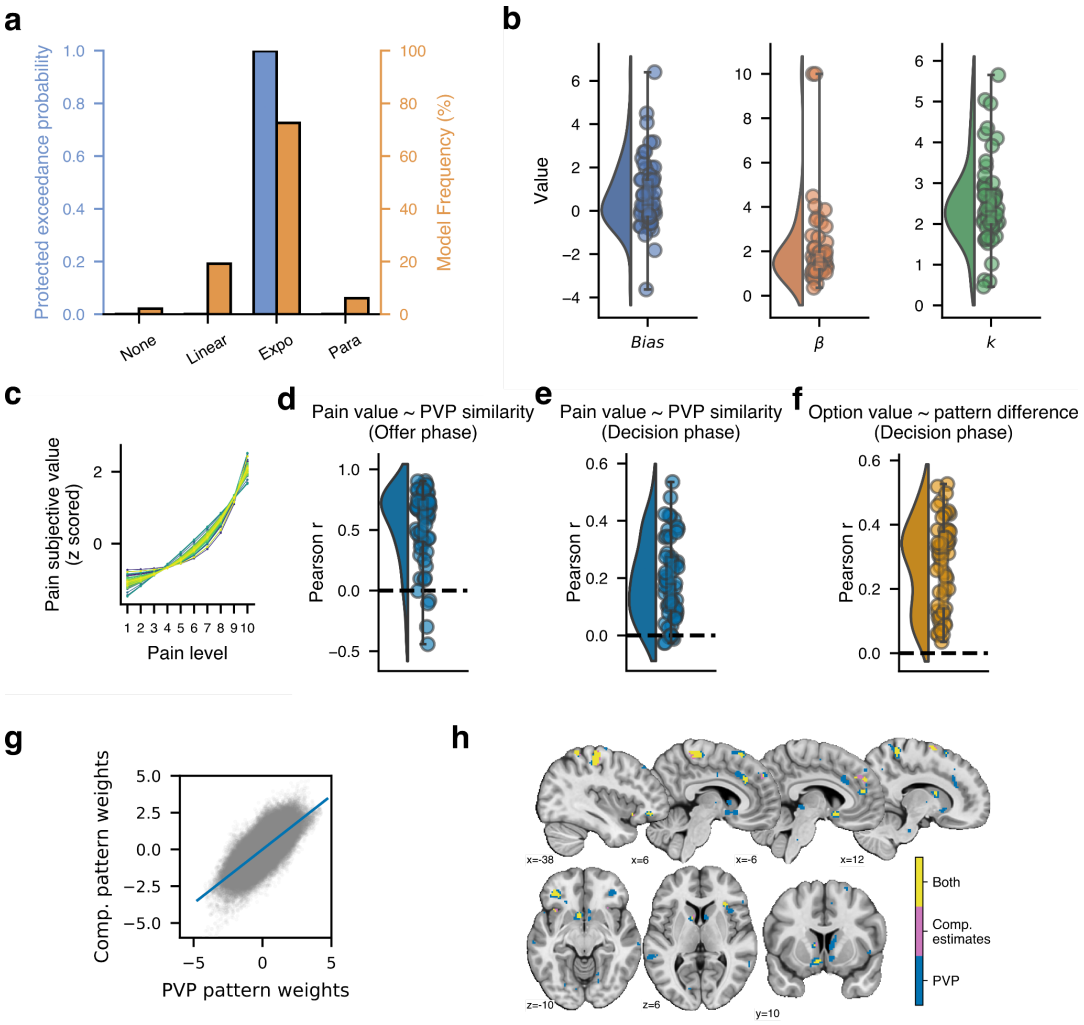


**Fig. S3. Results from the computational modelling of behaviour. (a)** Model comparison results indicating that the exponential scaling of pain was the best model for most participants. **(b**) Distribution of parameters for the scaling and choice functions for the winning exponential model (see Vogel et al., 2021). **(c)** Relationship between pain levels and the estimated pain value using the exponential model for each participant **(d)** Distribution of correlations between the estimated pain value and PVP similarity within participants for the offer phase. **(e)** Same as d for the decision phase. **(f)** Distribution of the relationships between the option value (pain value - money value) and the difference in PVP and MVP similarity at each trial within participants. **(g)** Relationship between the weights of the multivariate pattern predicting computational estimates of pain value and the weights of the PVP. **(h)** Distinction (blue, purple) and overlap (yellow) between the bootstrap corrected ($p < 0.001$) weights of the multivariate pattern predicting computational estimates of pain value and the weights of the PVP.

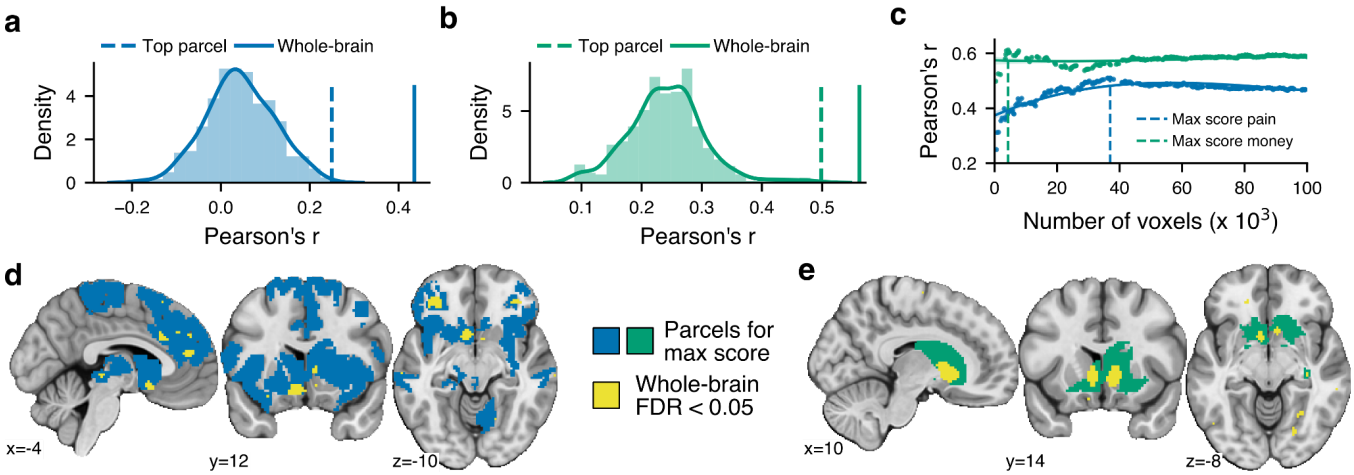


**Fig. S4. Local prediction of future pain and money levels. (a-b)** Distribution of the Pearson correlation coefficient between the actual and predicted level in 486 parcels for **(a)** the future pain level and **(b)** the level of money offered. **(c)** Pearson correlations between actual and predicted levels as a function of the number of voxels in the prediction for future pain (blue) and money (green). **(d-e)** Brain maps showing the parcels included in the maximal prediction shown in c (blue/green) and the thresholded whole-brain pattern (yellow) for **(d)** pain offer level and **(e)** money offer level.

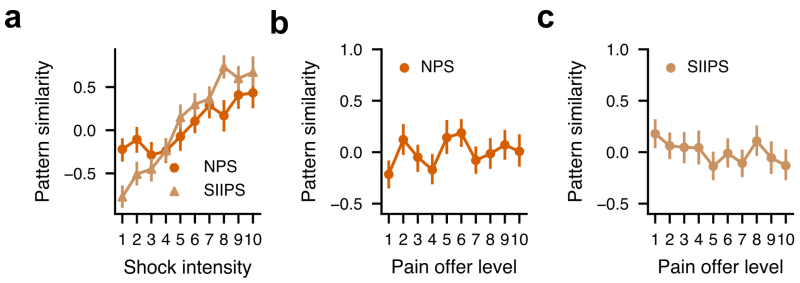


**Fig. S5. (a)** Average z-scored pattern similarity between the shock intensity levels and previously developed patterns predicting pain experience. **(b)** Pattern similarity between the NPS and activity for each level of pain offered. **(c)** Pattern similarity between the SIIPS and activity for each level of pain offered.

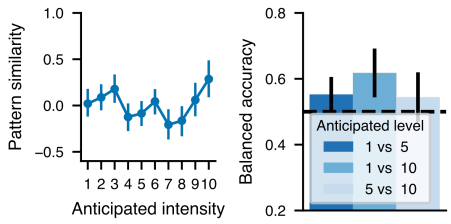


**Fig. S6.** Pattern similarity (left) and binary classification accuracies (right) obtained when applying the PVP to the Anticipation phase of the task.

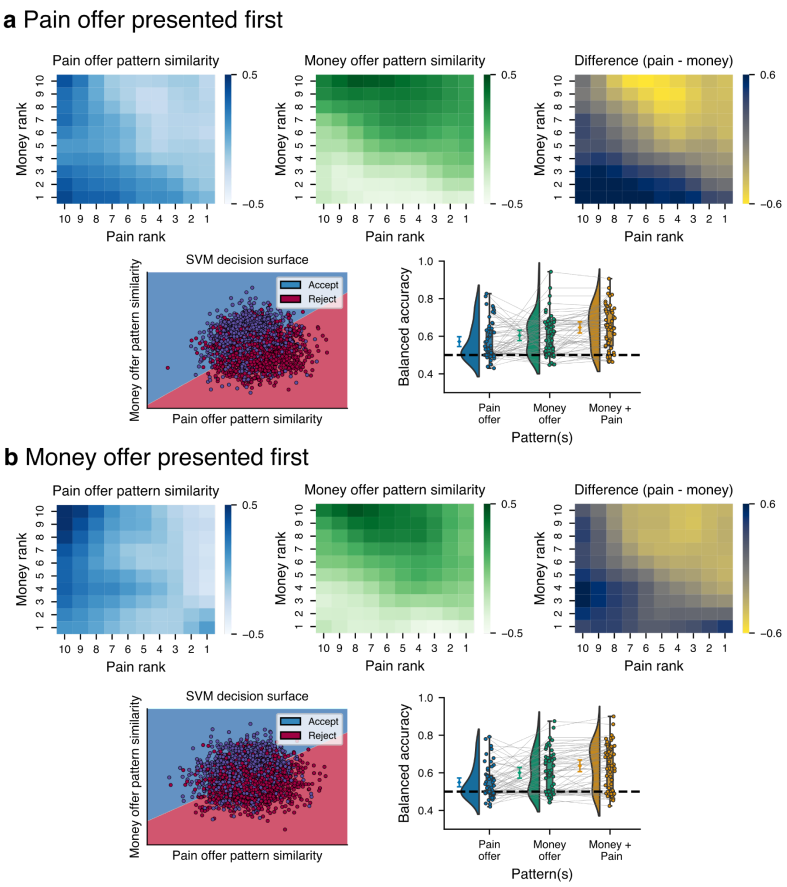


**Fig. S7.** Prediction of participants' decisions using pain and money multivariate patterns for trials in which the pain intensity was presented first **(a)** and trials in which the monetary amount was presented first **(b)**. Caption for the figure is the same as Figure 4 in the main text.

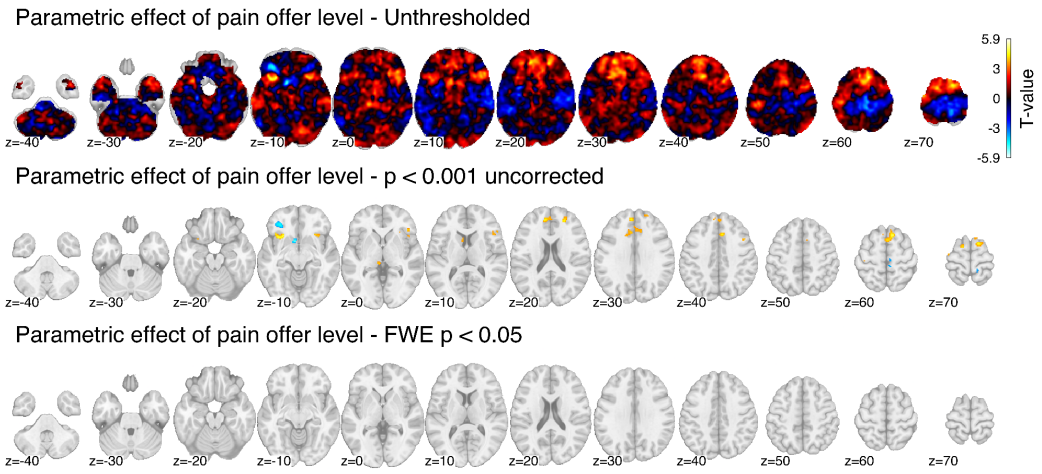


**Fig. S8. Univariate parametric response to pain level.** The pattern is shown untresholded (top), thresholded at p < 0.001, uncorrected (middle) and at p < 0.05, FWE corrected (bottom). The color bar shows t-scores from a one-sample t-test.

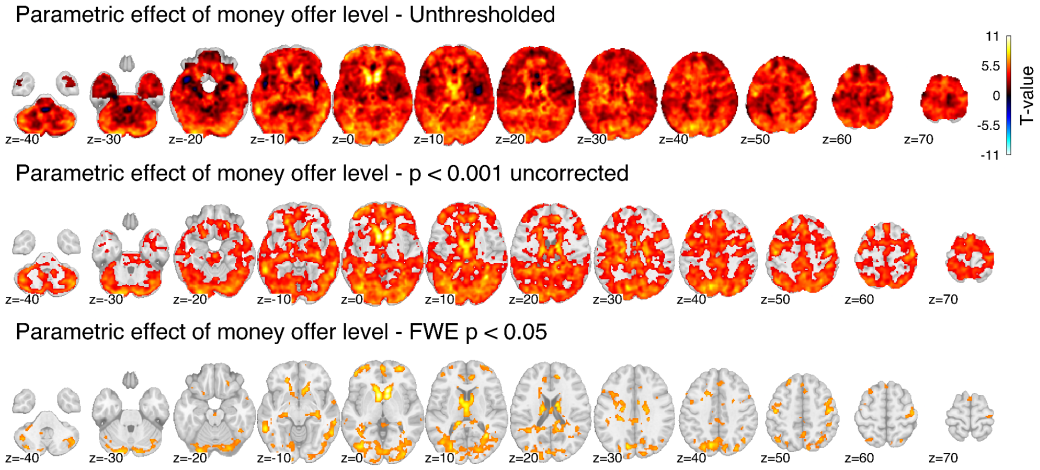


**Fig. S9. Univariate parametric effect of money level.** The pattern is shown untresholded (top), thresholded at p < 0.001, uncorrected (middle) and at p < 0.05, FWE corrected (bottom). The color bar shows t-scores from a one-sample t-test.

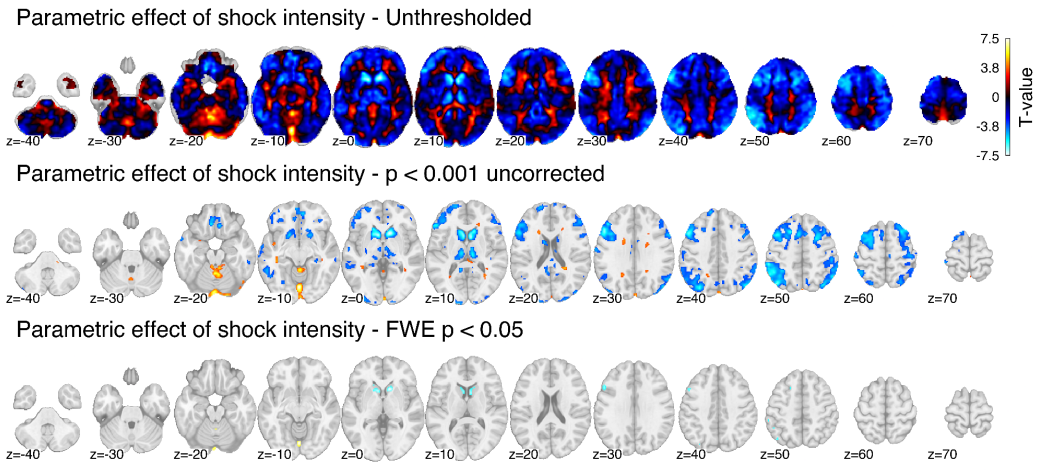


**Fig. S10. Univariate parametric response to shock intensity.** The pattern is shown untresholded (top), thresholded at p < 0.001, uncorrected (middle) and at p < 0.05, FWE corrected (bottom). The color bar shows t-scores from a one-sample t-test.

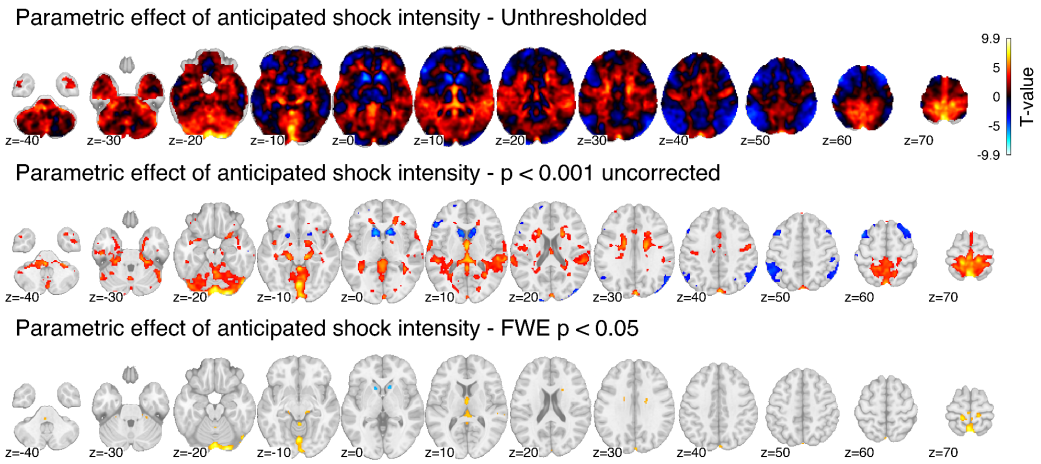


**Fig. S11.** Univariate parametric response to anticipated shock intensity. The pattern is shown untresholded (top), thresholded at p < 0.001, uncorrected (middle) and at p < 0.05, FWE corrected (bottom). The colorbar shows t-scores from a one-sample t-test.

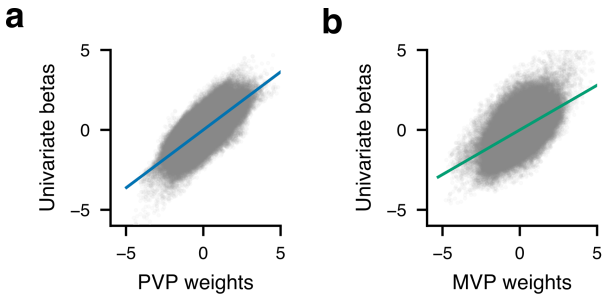


**Fig. S12.** **(a)** Spatial correlation between the standardized univariate parametric effect of pain level and the standardized weights of the pain value pattern. **(b)** Spatial correlation between the standardized univariate parametric effect of money level and the standardized weights of the money value pattern

## References


1. O Esteban, et al., fMRIPrep: a robust preprocessing pipeline for functional MRI. *Nat. Methods* (2018).

2. O Esteban, et al., fmriprep. *Software* (2018).

3. K Gorgolewski, et al., Nipype: a flexible, lightweight and extensible neuroimaging data processing framework in python. *Front. Neuroinformatics* **5**, 13 (2011).

4. KJ Gorgolewski, et al., Nipype. *Software* (2018).

5. NJ Tustison, et al., N4itk: Improved n3 bias correction. *IEEE Transactions on Med. Imaging* **29**, 1310–1320 (2010).

6. B Avants, C Epstein, M Grossman, J Gee, Symmetric diffeomorphic image registration with cross-correlation: Evaluating automated labeling of elderly and neurodegenerative brain. *Med. Image Analysis* **12**, 26–41 (2008).

7. Y Zhang, M Brady, S Smith, Segmentation of brain MR images through a hidden markov random field model and the expectation-maximization algorithm. *IEEE Transactions on Med. Imaging* **20**, 45–57 (2001).

8. V Fonov, A Evans, R McKinstry, C Almli, D Collins, Unbiased nonlinear average age-appropriate brain templates from birth to adulthood. *NeuroImage* **47, Supplement 1**, S102 (2009).

9. M Jenkinson, P Bannister, M Brady, S Smith, Improved optimization for the robust and accurate linear registration and motion correction of brain images. *NeuroImage* **17**, 825–841 (2002).

10. RW Cox, JS Hyde, Software tools for analysis and visualization of fmri data. *NMR Biomed*. **10**, 171–178 (1997).

11. MF Glasser, et al., The minimal preprocessing pipelines for the human connectome project. *NeuroImage* **80**, 105–124 (2013).

12. M Jenkinson, S Smith, A global optimisation method for robust affine registration of brain images. *Med. Image Analysis* **5**, 143–156 (2001).

13. DN Greve, B Fischl, Accurate and robust brain image alignment using boundary-based registration. *NeuroImage* **48**, 63–72 (2009).

14. JD Power, et al., Methods to detect, characterize, and remove motion artifact in resting state fmri. *NeuroImage* **84**, 320–341 (2014).

15. Y Behzadi, K Restom, J Liau, TT Liu, A component based noise correction method (CompCor) for BOLD and perfusion based fmri. *NeuroImage* **37**, 90–101 (2007).

16. TD Satterthwaite, et al., An improved framework for confound regression and filtering for control of motion artifact in the preprocessing of resting-state functional connectivity data. *NeuroImage* **64**, 240–256 (2013).

17. C Lanczos, Evaluation of noisy data. *J. Soc. for Ind. Appl. Math. Ser. B Numer. Analysis* **1**, 76–85 (1964).

18. A Abraham, et al., Machine learning for neuroimaging with scikit-learn. *Front. Neuroinformatics* **8** (2014).

19. Vogel, T. A., Savelson, Z. M., Otto, A. R., & Roy, M. (2020). Forced choices reveal a trade-off between cognitive effort and physical pain. ELife, 9, e59410. https://doi.org/10.7554/eLife.59410

20. Rigoux, L., Stephan, K. E., Friston, K. J., & Daunizeau, J. (2014). Bayesian model selection for group studies—Revisited. NeuroImage, 84, 971–985. https://doi.org/10.1016/j.neuroimage.2013.08.065

21. B Petre, et al., Evoked pain intensity representation is distributed across brain systems: A multistudy mega-analysis. *bioRxiv* p. 2020.07.04.182873 (2020) Publisher: Cold Spring Harbor Laboratory Section: New Results.

22. TD Wager, et al., An fMRI-Based Neurologic Signature of Physical Pain. *New Engl. J. Medicine* **368**, 1388–1397 (2013) Publisher: Massachusetts Medical Society _eprint: https://doi.org/10.1056/NEJMoa1204471.

23. CW Woo, et al., Quantifying cerebral contributions to pain beyond nociception. *Nat. Commun*. **8** (2017).